International Journal of Solids and Structures 46 (2009) 2453–2462

Contents lists available at ScienceDirect

International Journal of Solids and Structures

journal homepage: www.elsevier.com/locate/ijsolstr

A cohesive zone model for fatigue crack growth allowing for crack retardation ☆

Ani Ural [a], Venkat R. Krishnan [b], Katerina D. Papoulia [c,*]

[a] Department of Mechanical Engineering, Villanova University, 800 Lancaster Avenue, Villanova, PA 19085, USA
[b] Department of Theoretical and Applied Mechanics, 217 Kimball Hall, Cornell University, Ithaca, NY 14853, USA
[c] Department of Civil and Environmental Engineering, University of Waterloo, Waterloo, Ont., Canada N2L 3G1

ARTICLE INFO

Article history:
Received 3 October 2007
Received in revised form 14 November 2008
Available online 7 February 2009

Keywords:
Fatigue
Damage
Cohesive zone models
Crack propagation
Life prediction
Crack retardation
Healing
Mean stress effect
Load-ratio
Overload

ABSTRACT

A damage-based cohesive model is developed for simulating crack growth due to fatigue loading. The cohesive model follows a linear damage-dependent traction–separation relation coupled with a damage evolution equation. The rate of damage evolution is characterized by three material parameters corresponding to common features of fatigue behavior captured by the model, namely, damage accumulation, crack retardation and stress threshold. Good agreement is obtained between finite element solutions using the model and fatigue test results for an aluminum alloy under different load ratios and for the overload effect on ductile 316 L steel.

1. Introduction

The fatigue life of a structure is influenced by mechanical, microstructural and environmental factors, all of which result in material damage, typically equated to crack length (Miller, 1991). Indeed the field of fracture mechanics has had profound influence on fatigue analysis. For mechanical type loads, fatigue life of a component or structure is calculated as the number of loading cycles needed to grow a pre-existing crack to a predetermined critical dimension or to nucleate and grow a crack from a notch or other location of stress concentration.

The focus of this paper is the so-called stage-II fatigue crack growth, i.e., the stable propagation of a dominant crack. Starting with the Paris model (Paris and Erdogan, 1963; Paris et al., 1961), fatigue life predictions have typically been based on equations relating the stage-II rate of crack growth (da/dN) to the stress intensity range (ΔK), also called the driving force, characteristic of a constant magnitude cyclic applied load and of specimen geometry. Here a is the crack length and N is the number of loading cycles. Attempts to incorporate more complex conditions affecting the crack growth rate led to models whose parameters depend on characteristics of the applied load or of the environment, as well as the redefinition of ΔK.

The Paris model and similar approaches are valid under the ideal conditions of linear elastic fracture mechanics (LEFM), small-scale yielding, constant amplitude cyclic loading and long cracks. When these conditions are not met, these approaches lose their predictive capability. In particular, they are unable to model crack retardation due, for example, to roughness induced crack closure (Elber, 1971), oxidation, or the presence of a residual stress field (Noroozi et al., 2008).

We develop a cohesive zone model, i.e., a model of the traction–separation relationship ahead of the crack tip, capable of macroscopically modeling fatigue crack growth. Cohesive zone models can capture the nonlinear behavior occurring in the process zone provided that the latter can be considered as a zone of zero thickness. Since they can be paired with a plasticity model in the bulk material, they can be especially useful in simulating fatigue behavior of materials that violate small scale yielding assumptions at the crack tip. Their use in fracture problems has become common in recent years. Cohesive zone models are also useful when micromechanical processes acting at a scale smaller than the grid size used in the finite element analysis affect the rate of crack growth. The relevant micromechanics can then be incorporated in the cohesive zone model. This process is sometimes called "subgrid modeling".

☆ Supported in part by NASA Cooperative Agreement CC3-994, "Institute for Future Space Transport", NSF Award NMS-0239068, and NSERC research Grant 342117-07.

* Corresponding author. Tel.: +1 519 888 4567.
E-mail addresses: ani.ural@villanova.edu (A. Ural), vk67@cornell.edu (V.R. Krishnan), papoulia@uwaterloo.ca (K.D. Papoulia).

0020-7683/$ - see front matter © 2009 Elsevier Ltd. All rights reserved.
doi:10.1016/j.ijsolstr.2009.01.031

Examples are the interaction of asperities as a cause of crack closure and the effect of residual stresses when the plastic zone is not adequately resolved. A crack retardation mechanism as introduced in the proposed model can be used to capture these effects. Subgrid modeling is ideally carried out through multiscale analysis, which is not addressed in this paper. In that light, one could envision obtaining the parameters of the proposed model from micromechanical analysis at a smaller scale.

Cohesive zone fatigue models have most commonly been implemented as cohesive interface finite elements. de Andres et al. (1999) proposed a bilinear traction–separation relationship, which unloads to the origin with no cyclic degradation of either the stiffness or the peak traction. Nguyen et al. (2001) pointed out that such a model can lead to plastic shakedown that arrests crack growth after a few cycles. Hence, a distinction between loading and unloading paths is necessary, which allows for subcritical crack growth. In Nguyen et al. (2001), a cohesive model with an unloading–reloading hysteresis was developed. In this work, the stiffness and the peak load degrade proportionally to the unloading stiffness as the number of cycles increases. Roe and Siegmund (2001) introduced a damage variable, whose evolution resulted in the degradation of the cohesive zone traction. The cohesive relationship under monotonic loading was based on the potential proposed by Xu and Needlemanm (1994). Maiti and Geubelle (2005) proposed a cohesive model of fatigue fracture in polymeric materials in which the cohesive stiffness evolves as a function of the rate of opening displacement and of the number of loading cycles since the onset of failure. Crack retardation or healing due to artificial crack closure (a wedge introduced in the wake of the crack) was addressed by these authors in Maiti and Geubelle (2006). Maiti et al. (2006) incorporated healing kinetics at the atomic level for a class of self-healing materials.

The proposed cohesive zone model, an earlier form of which was presented in Ural and Papoulia (2004), is bilinear under monotonic loading and shows a degrading peak traction and stiffness behavior under cyclic loading due to an evolving damage variable. The model is a constitutive relationship of the material, i.e., unlike the Paris and other models, its parameters do not depend on loading characteristics such as the load ratio, defined as the ratio of minimum to maximum load. Rather, it contains three physically motivated parameters, which govern crack advance, threshold, and retardation, respectively. As in Roe and Siegmund (2001), the model introduces a scalar (energy like) damage variable, governed by an evolution equation, which provides a phenomenological framework to account for the nonlinear processes associated with fatigue failure. Special emphasis is placed on the ability of the model to capture crack retardation, which is known to depend on the load ratio. In particular, the damage variable can evolve nonmonotically; a decrease in damage partially restores the strength of the material and therefore retards crack growth. However, we do not specifically attribute crack retardation to any of the possible physical mechanisms mentioned earlier, namely roughness induced crack closure or the effect of residual stresses. Indeed, crack retardation and damage nonmonotonicity could even correspond to physical crack healing. Several recent proposals have been made for self-healing structural materials (White et al., 2001; Toohey et al., 2007). Regardless of the physical mechanism, we show that the model captures the effect of mean stress (load ratio) and of overload.

The remainder of the paper is organized in the following manner. Section 2 presents the details of the proposed cohesive model. Section 3 includes a mathematical analysis of well-posedness of the model. Section 4 presents aspects of the finite element implementation and some preliminary testing. In Section 5, the predictive capability of the proposed model is evaluated through two dimensional finite element simulations of cyclic fatigue tests of A356-T6 compact-tension (CT) specimens at two load ratios. Section 6 illustrates the ability of the model to capture the effect of overload.

2. A damage-based cohesive model allowing for crack retardation

We postulate a degrading linear traction–separation relationship of the form

$$T = F(\kappa)\delta, \tag{1}$$

where κ is a damage variable, δ is the effective opening displacement, defined in Section 4, and T is a scalar effective cohesive traction, also defined in Section 4.

The dependence of the elastic coefficient F on κ is specified by

$$F(\kappa) = \frac{\sigma_c(1-\kappa)}{\kappa(\delta_u - \delta_c) + \delta_c}; \tag{2}$$

δ_c is the critical displacement at which the crack initiates and damage starts to accumulate, δ_u is the failure displacement, i.e., the displacement at which the traction becomes zero, and σ_c is the initial peak traction of the interface. The traction T is also required to satisfy the inequality $T \leqslant C(\kappa)$, where $C(\kappa)$ is specified by

$$C(\kappa) = \sigma_c(1-\kappa). \tag{3}$$

Under cyclic loading, the model exhibits a degrading peak traction, i.e., a decreasing value of $C(\kappa)$, and a degrading stiffness, i.e., a decreasing value of $F(\kappa)$ as the value of κ increases (Fig. 1), resulting in eventual loss of load transmission ability of the interface. The variable κ takes values between 0 and 1 corresponding to no damage and complete fracture, respectively. The expression proposed in (2) has the desirable property that the elastic coefficient $F(\kappa)$ is strictly decreasing so that the traction T decreases from σ_c (when $\kappa = 0$) to 0 (when $\kappa = 1$). The ascending and descending linear branches of the monotonic response are not explicitly defined by the above equations but rather are a consequence of these equations. On the ascending branch, the relationship $T = F(\kappa)\delta$ holds with $\kappa = 0$ and hence $F(\kappa)$ is a fixed constant. Therefore, the relation between T and δ is linear on the ascending branch.

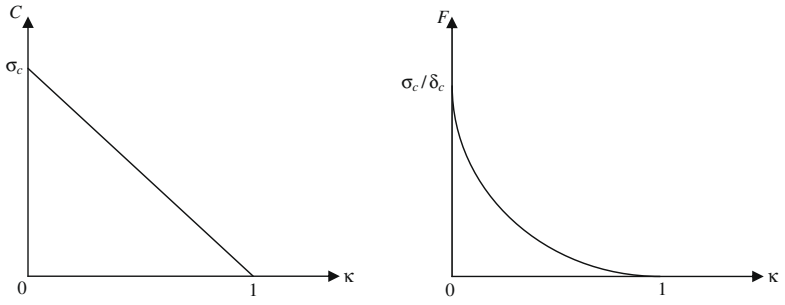

Fig. 1. Evolution of peak traction (left) and stiffness (right) with accumulation of damage.

When the opening displacement is increasing and T is at its capacity (i.e., the critical traction σ_c is attained), the inequality $T \leqslant C(\kappa)$ becomes binding and the equation $F(\kappa)\delta = C(\kappa)$, arrived at by substituting $T = C(\kappa)$ into (1), holds. Upon substituting (2) and (3), this yields $\delta = \kappa(\delta_u - \delta_c) + \delta_c$. Thus, the choice of (2) results in a linear relationship between κ and δ on this branch of the loading curve. Furthermore, substituting (3) shows that T, κ, and δ are all linearly related. Fig. 2 shows a schematic representation of the proposed cohesive traction–displacement relationship. In this figure, branch OB is the ascending part of the loading curve, BC is the descending part of the loading curve, and CO is the unloading curve.

The evolution of the damage variable is governed by:

$$\begin{aligned} &\dot{\kappa} = \alpha^* \kappa (T - \beta C)(\dot{\delta}) && \text{if } (T - \beta C)(\dot{\delta}) > 0, \\ &\dot{\kappa} = 0 && \text{if } (T - \beta C)(\dot{\delta}) < 0, \\ &\dot{\kappa} = \dot{\lambda} && \text{if } T = C \text{ and } \dot{\delta} > 0, \end{aligned} \tag{4}$$

where $\dot{\lambda}$ is a free variable, and α^*, β are material parameters that capture the rate of damage evolution, and the threshold for initiation of damage, respectively. The parameter α^* takes on one of two distinct values for the cases of loading and unloading, $\dot{\delta} > 0$ or $\dot{\delta} < 0$, denoted by the parameters α and $-\gamma$, respectively, which are regarded as material parameters.

Evolution Eq. (4) are reminiscent of damage plasticity (Lubliner et al., 1989). The first and second equations allow damage accretion (when $\dot{\delta} > 0$) or healing (when $\dot{\delta} < 0$) to occur only when the traction is greater or less than the threshold limit during loading and unloading, respectively. Physically, this can be thought of as damage accretion or healing occurring only when the work done by an effective traction, i.e., the value of the traction above the threshold, on the crack surface is positive. A key property of both surface roughness and crack tip plasticity as causes of crack retardation is that they become strongly active only when the crack opening displacement returns to a small value in the trough of the cyclic loading. This explains why our evolution equation for damage decrease is inactive until the traction drops below a threshold level. During loading, if the value of the traction (T) reaches peak traction (C), it is constrained to move along the envelope $T = C(\kappa)$. This in turn forces the relationship $C(\kappa) = F(\kappa)\delta$ to hold, which defines the evolution of κ. Therefore, for this situation, the third case of (4) does not constrain $\dot{\kappa}$ at all since $\dot{\lambda}$ is free. This case is again analogous to classical plasticity theory in which a parameter $\dot{\lambda}$ is chosen in the loading case to ensure that the stress remains on the yield surface. The analogy to plasticity is not complete, however, because our model does not involve a strain or relative displacement decomposition.

Accordingly, when the traction–displacement relationship is tracing the descending branch of the monotonic cohesive curve, the evolution of damage is governed by the plasticity parameter λ, and it is only a function of the current opening displacement. However, during reloading, damage depends on the rate of deformation, previous damage accumulation, cohesive traction and fatigue threshold. During unloading, the value of κ can decrease if the traction is lower than the threshold. Decrease of the damage variable during unloading, controlled by the model parameter γ, is a vehicle to capture crack retardation. In addition, a penalty stiffness is included in the formulation of the model for negative displacement values to prevent interpenetration of the crack faces.

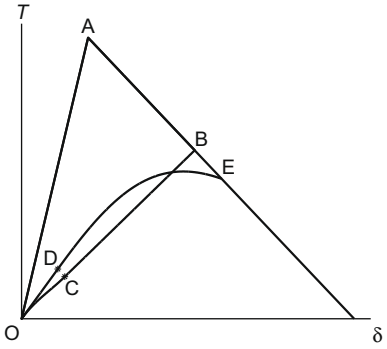

Fig. 2. Schematic representation of the proposed cohesive traction–separation relationship. No change in damage occurs during OA; damage starts increasing after the threshold at A; BC shows the descending part of the loading curve; no damage change takes place during the unloading path CD; damage decreases during unloading from D to O.

3. Well-posedness conditions

The model has some obvious restrictions on the parameter values such as $\alpha \geqslant 0$, $0 < \beta < 1$ and $\gamma \geqslant 0$. In this section, we will also derive two subtler conditions that are necessary for the model to be well posed mathematically.

The first condition concerns the case that the current state of the interface is very close to, but not exactly on, the descending linear branch. In this case, for the model to be well posed, the interface should evolve so that the state tends toward the descending linear branch. If it tends away from the branch, this creates an ill-behaved model since it implies that a small perturbation to the state can cause a large deviation in subsequent trajectory. First, consider a point on the descending branch of the model. Such a point has $F(\kappa)\delta = C(\kappa)$, and thus satisfies $\delta = \kappa(\delta_u - \delta_c) + \delta_c$. The slope $dT/d\delta$ in this case is seen to be $-\sigma_c/(\delta_u - \delta_c)$ (independent of κ and δ). Next, consider a point satisfying $\delta = \kappa(\delta_u - \delta_c) + \delta_c - \epsilon$, where $\epsilon > 0$ is extremely small. In this case, $T = F(\kappa)\delta < C(\kappa)$ so the point is below the descending branch, but only slightly. The condition for well-posedness in this case is that $dT/d\delta \geqslant -\sigma_c/(\delta_u - \delta_c)$, i.e., the slope of the trajectory from this point should not be less than the slope of a nearby point on the descending branch. For a point not on the descending branch, when loading is applied (i.e., $\dot{\delta} > 0$), we have

$$\frac{dT}{d\delta} = \frac{d(F(\kappa)\delta)}{d\delta} \tag{5}$$

$$= F'(\kappa)\frac{d\kappa}{d\delta}\delta + F(\kappa) \tag{6}$$

$$= F'(\kappa)\alpha\kappa(T - \beta C)\delta + F(\kappa). \tag{7}$$

Note that we used the equation $\dot{\kappa} = \alpha\kappa(T - \beta C)\dot{\delta}$ (which is the first equation of (4) when $\dot{\delta} > 0$) to obtain $d\kappa/d\delta$. By using the relationship $\delta = \kappa(\delta_u - \delta_c) + \delta_c - \epsilon$ and eventually dropping the ϵ, simplifying and rearranging one obtains the following inequality:

$$\alpha \leqslant \frac{1}{\sigma_c \kappa(1-\kappa)(1-\beta)(\delta_u - \delta_c)}. \tag{8}$$

This inequality must hold for all values of κ. The denominator is maximized when $\kappa = 1/2$, so a sufficient condition that implies the above inequality is simply

$$\alpha < \frac{4}{\sigma_c(\delta_u - \delta_c)(1-\beta)}. \tag{9}$$

The second well-posedness condition concerns the healing part of the curve. If the healing effect is too strong, then the material may exhibit a descending branch during healing, i.e., a negative value of $dT/d\delta$, which seems unphysical and is likely to increase numerical problems. We have

$$\frac{dT}{d\delta} = \frac{d(F(\kappa)\delta)}{d\delta} \tag{10}$$

$$= F'(\kappa)\frac{d\kappa}{d\delta}\delta + F(\kappa) \tag{11}$$

$$= F'(\kappa)\gamma\kappa(\beta C - T)\delta + F(\kappa). \tag{12}$$

Substituting the above formula into the condition $dT/d\delta \geqslant 0$, simplifying and rearranging yields the condition

$$\gamma \leqslant \frac{1}{\frac{\sigma_c \delta_u \kappa}{\kappa(\delta_u-\delta_c)+\delta_c}\left(\beta - \frac{\delta}{\kappa(\delta_u-\delta_c)+\delta_c}\right)\delta}. \tag{13}$$

This must hold for all κ, δ such that $T \leqslant \beta C$. Treating δ as a free variable, the denominator of the above formula is maximized when $\delta = \beta(\kappa(\delta_u - \delta_c) + \delta_c)/2$. Substitute this into (13) to obtain the following inequality, which is sufficient to imply (13):

$$\gamma \leqslant \frac{4}{\sigma_c \delta_u \kappa \beta^2}. \tag{14}$$

The worst case is when $\kappa = 1$, and thus the sufficient condition for the second well-posedness criterion is that

$$\gamma \leqslant 4/(\sigma_c \delta_u \beta^2). \tag{15}$$

4. Finite element implementation and preliminary testing

The cohesive model described in Section 2 is implemented as a constitutive relationship governing interface elements in a finite element mesh. These are zero thickness elements obtained by duplicating grid points along bulk element edges. Our cohesive finite element implementation, which is based in part on work by Ortiz and Pandolfi (1999), depends on an effective scalar parameter

$$\delta = \sqrt{\eta^2 \boldsymbol{\delta}_s \cdot \boldsymbol{\delta}_s + \delta_n^2}, \tag{16}$$

where η is a nondimensional factor that couples the normal and shear effects, $\boldsymbol{\delta}_s$ is the shear component of the opening displacement and δ_n is the normal component. The cohesive model (1) defines a scalar traction T as a function of effective opening displacement. This scalar traction is used in turn to define the usual vector traction via the formula:

$$\mathbf{t} = \frac{T}{\delta}(\eta^2 \boldsymbol{\delta}_s + \delta_n \mathbf{n}). \tag{17}$$

Following standard procedures, e.g., Xu and Needlemanm (1994), Ortiz and Pandolfi (1999), the finite element discretization is obtained from a virtual power equation that involves power due to stresses in the bulk material and power due to interface tractions.

Because of the ascending branch of the cohesive model, which makes the model active before the critical stress is reached, node duplication is necessary from the outset of the simulation. In cases where the crack path is not known in advance, cohesive interface elements must tile the domain. This results in mesh dependence associated with the ascending stiffness of the cohesive model (Klein et al., 2000). On the other hand, implementation of cohesive interface elements that are inactive (rigid) before the critical stress is reached (Ortiz and Pandolfi, 1999; Papoulia et al., 2003), and therefore can be inserted adaptively as needed, is not easy in implicit calculations. However, all applications in this paper involve a predetermined crack path so that cohesive interface elements are inserted along that path only and the effect of the ascending stiffness is minimal. Likewise, the obvious mesh dependence of interface finite elements is avoided without need of any special meshing strategies (Papoulia et al., 2006). Some algorithmic details of implementing the proposed fatigue fracture model within this framework are presented in the Appendix.

As an example, a double cantilever beam (DCB) geometry is used to show damage accumulation and crack growth according to the model. The DCB geometry results in mode I crack growth. The crack is constrained to grow along the centerline of the specimen. The bulk material is aluminum with material properties E = 70,000 MPa and $\nu = 0.33$. The cohesive model parameters chosen are $\sigma_c = 6.66$ MPa, $\eta = 0.5$ and $\delta_c = 0.203$ mm. The parameters β and γ are taken to be zero. The finite element mesh, shown in Fig. 3, consists of 1600 plane strain elements and 100 cohesive interface elements inserted along the centerline from the initial crack tip to the free end of the specimen. Due to symmetry, only half the specimen is modeled. A displacement of constant amplitude equal to 6 mm is applied and cycled 115 times. Fig. 4 shows crack growth against number of load cycles. As a result of this loading, damage as measured by the damage variable κ accumulates, resulting in a degrading traction–separation curve. Fig. 5 shows the traction–separation evolution to fracture in the first cohesive element. The accumulation of damage eventually results in fracture of the cohesive element. In the figure, each loop of the simulation results in a lower traction because the damage variable κ increases from loop to loop, hence $F(\kappa)$ decreases. By cycle 55, $\kappa = 1$ and $F(\kappa) = 0$. The capacity $C(\kappa)$ is not attained for most of

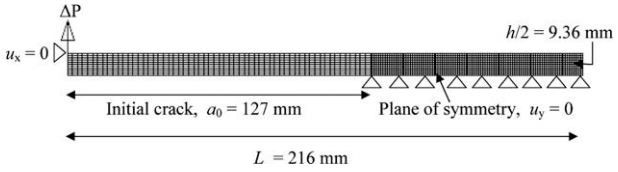

Fig. 3. Mesh for the DCB model.

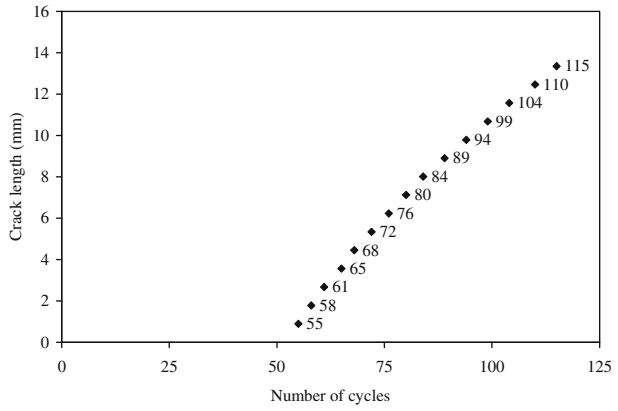

Fig. 4. Fatigue crack growth in the DCB model vs. number of applied load cycles. Number given next to a data point indicates the cycle number, at which crack propagation at that level occurs.

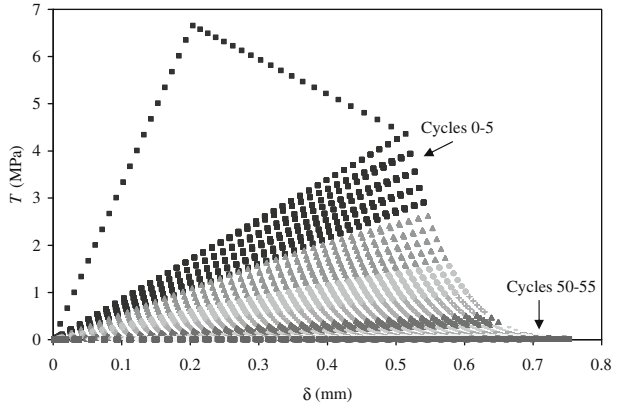

Fig. 5. Traction vs. relative displacement curve for the first cohesive element in the DCB specimen. Each gray-level represents a five-cycle interval. Fracture of the element occurs at the 55th cycle.

the loops and hence the descending branch does not exhibit its linear envelope. This is because the simulation incorporates fixed-amplitude displacement loading rather than fixed-amplitude force loading, so the crack mouth opening displacement (CMOD) never exceeds a certain fixed δ even when the interface is fully ruptured.

5. Simulations of fatigue tests of A356-T6 compact tension specimens

We simulate fatigue tests performed on A356-T6 cast aluminum alloy CT specimens with a thickness of 9.1 mm for load ratios, R, equalling 0.1 and 0.5 under constant amplitude loading (Stephens, 1988). Fig. 6 shows the specimen dimensions. The loading and initial pre-crack locations of the specimens for the two R ratios are given in Table 1. During these tests, incremental crack growth lengths and the corresponding number of cycles were recorded. A definite R ratio effect in the test results was reported in detail.

In order to simulate the above fatigue experiments using the proposed model, the local cohesive strength of the material (σ_c) and work of separation per unit area (G_c) as well as bulk material properties were determined from axial cylindrical tests and fracture tests of A356-T6 aluminum alloy CT specimens, also reported

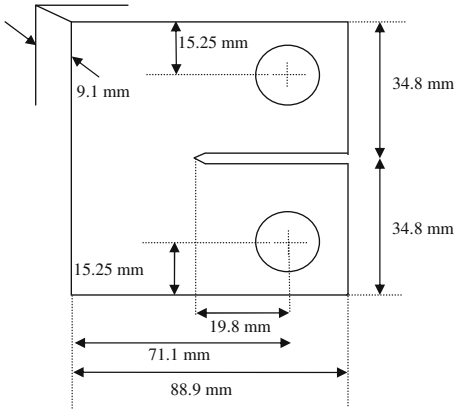

Fig. 6. CT specimen for fatigue tests.

Table 1
Initial and final locations of crack in CT test specimens and magnitude of fatigue loading applied to the specimens.

Loading	P_{min} (N)	P_{max} (N)	a_0 (mm)	a_f (mm)
$R = 0.1$	414.444	4144.444	23	38
$R = 0.5$	1615	3230	30	45

in Stephens (1988). Besides providing elastic properties $E = 70,000$ MPa, $\nu = 0.33$, the axial cylindrical tests also produced bounds for the yield stress σ_y and the critical stress σ_c of the material. The yield stress was required to take values between the stress at which the material started to deviate from linearity, 180 MPa, and the stress corresponding to 0.2% strain, 229 MPa. The critical stress was required to lie between the yield stress and the ultimate stress, 289 MPa. The values of these properties used to simulate the fatigue experiments were $\sigma_c = 190$ MPa and $G_c = 5.50$ N/mm. These were chosen by fitting the proposed model to load vs. crack mouth opening displacement (CMOD) monotonic curves obtained from fracture toughness tests of CT specimens (Ural, 2004). The bulk material was defined as a plastic material with $\sigma_y = 180$ MPa and various amounts of hardening. The latter did not affect the life prediction calculations.

The location of cohesive interface elements, placed in the direction of crack growth, and the fatigue starter notch in the CT specimen are marked in Fig. 7. The finite element mesh used was composed of 13,080 quadrilateral elements and 60 cohesive interface elements and is shown in the undeformed and deformed configurations in Fig. 7. Under the assumption of plane strain, the estimated cohesive zone size can be calculated as de Andres et al. (1999)

$$r_{coh} = \frac{\pi}{8}\frac{E}{1-\nu^2}\frac{G_c}{\sigma_c^2}, \tag{18}$$

which gives a cohesive zone size of 4.7 mm. According to this calculation, the cohesive zone is spanned by approximately 7–8 interface elements. Increasing the number of interface elements in the cohesive zone did not affect the results. This indicates that the size of the interface elements was small enough to resolve the cohesive zone.

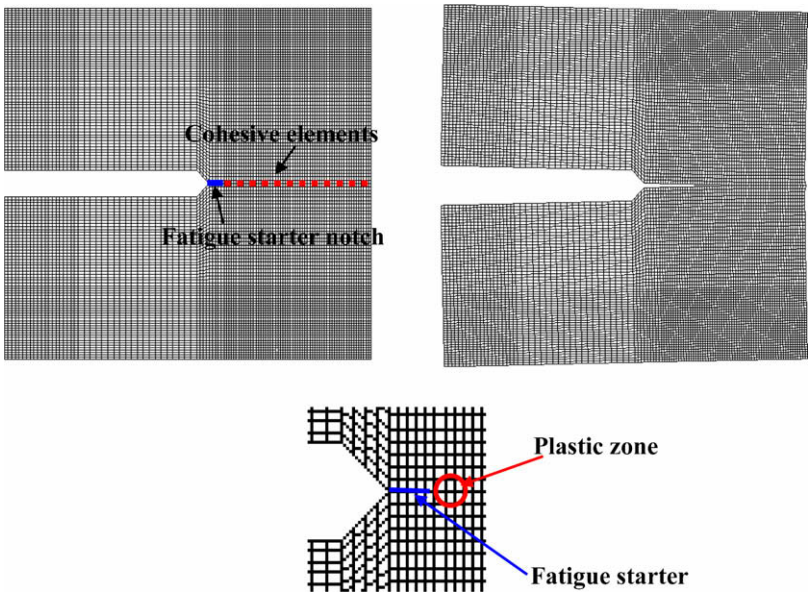

Fig. 7. Undeformed finite element mesh of CT specimen (top left), deformed mesh at the end of the simulations (top right), and close-up of the notch tip region (bottom). The displacement magnification factor is 5.

Cycle-by-cycle simulations of high-cycle fatigue applications require excessive computational resources. For this reason, a simple but quite effective extrapolation scheme was used to predict the fatigue life of the specimens. Suppose one wishes to simulate N cycles of a material whose fatigue parameters in our model are (α, β, γ). Suppose also that a damage-accumulation scaling function $f(k)$ exists such that one could instead compute only N/k cycles explicitly using modified parameters $(\alpha f(k), \beta, \gamma f(k))$. The function $f(k)$ is chosen so that one cycle with these modified parameters causes an equal amount of fatigue crack propagation as k cycles with the actual parameters. Note that the damage accumulation parameters α and γ are scaled but not the threshold parameter β. We carried out a variety of experiments with ranges of parameters and crack lengths and found that in all cases, linear scaling with $f(k) = k$ gave excellent results, i.e., N cycles with (α, β, γ) gave very similar results as N/k cycles with $(\alpha k, \beta, \gamma k)$. Note that the scaling is purely an extrapolation scheme and is not a change of the model parameters.

The model was implemented in the finite element software Abaqus. All analyses were performed under the assumption of plane strain. Each explicit cycle for the $R = 0.1$ simulation had 18 time steps and the $R = 0.5$ simulation had 10 time steps per load cycle. This was chosen so that each load step is an increment or decrement of 10% of the peak load. The fatigue parameters α, β, and γ that appear in the damage evolution Eq. (4) were chosen so that good agreement is obtained with the experimental crack length versus load cycle curves.

Figs. 8 and 9 show simulation and experimental crack length versus load cycle curves for the $R = 0.1$ and $R = 0.5$ tests, respectively. Parameters $\alpha = 0.000062$, $\beta = 0.17$, and $\gamma = 0.0002$ were used for both the $R = 0.1$ and $R = 0.5$ simulations. Good agreement was obtained with the fatigue crack growth test data. The results for $R = 0.5$ closely match the crack growth versus number of cycles experimental data. The results for $R = 0.1$ also show good agreement. The graphs show simulation results up to the onset of unstable crack growth as observed in the tests. The instability points predicted by the simulations are very close to the experimentally observed values. Table 2 shows the comparison between predicted and experimentally obtained initiation and failure cycles.

Based on the observations of Stephens (1988), roughness induced crack closure appears to be the crack retardation mechanism in these experiments. This was concluded from the change in linearity of load versus crack mouth opening displacement plots (CMOD) and fractography of the crack surfaces. The CMOD measurements indicated closure effects were present for $R = 0.1$ but not for $R = 0.5$. Fractography observations, on the other hand, indicated that some crack closure might be present in the $R = 0.5$ tests as evidenced by the smooth surfaces close to the pre-crack, which

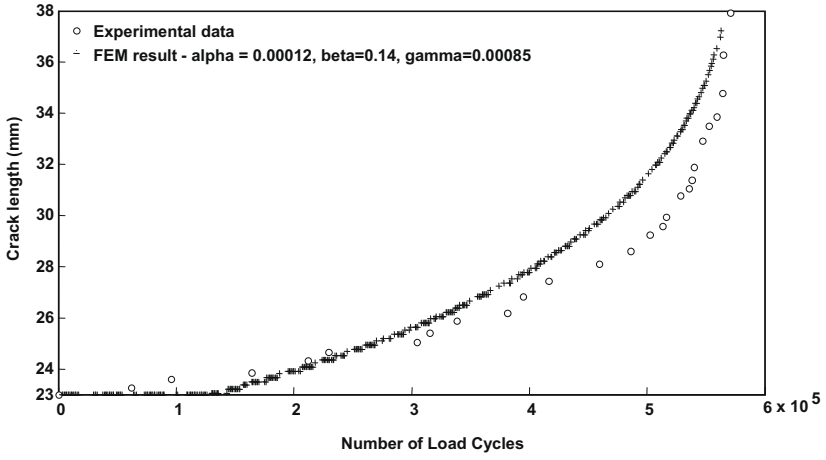

Fig. 8. Fatigue crack growth simulation results that best fit the test data for $R = 0.1$ loading.

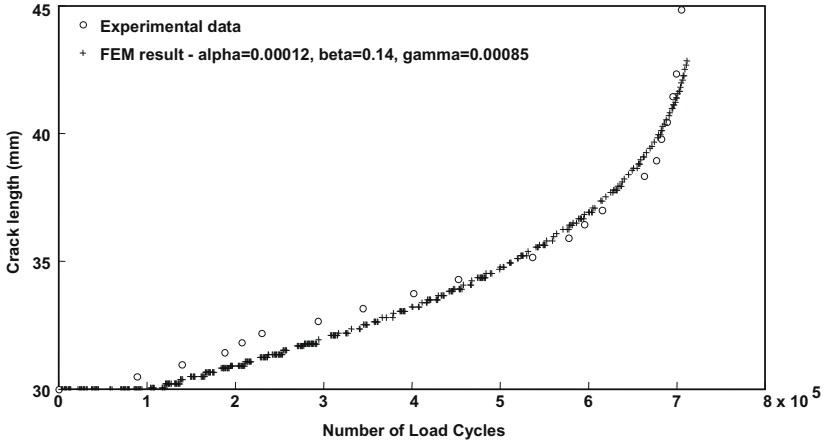

Fig. 9. Fatigue crack growth simulation results that best fit the test data for $R = 0.5$ loading.

Table 2
Initiation and failure cycles from tests and simulations for both R ratios.

Loading	Initiation cycle	Failure cycle
$R = 0.1$, simulation	117000	579000
$R = 0.1$, test	61853	570830
$R = 0.5$, simulation	98000	737000
$R = 0.5$, test	89050	705440

were assumed to be a result of fretting. Further, the crack growth plane changed very often during testing and the fracture surfaces showed an overall coarseness for both R ratios. It was reported in Stephens (1988) that the materials used in the tests had a very coarse microstructure. Still, roughness induced crack closure is mostly observed at low ΔK and R, which result in small crack tip opening displacements, comparable to the average height of the asperities (Suresh, xxx). Plasticity-induced crack closure was not considered to have a significant effect on the tests due to the low ductility of the material. It was also observed from the test data that the fatigue threshold for this material decreased with increasing R ratio. This is in agreement with previously obtained test data that show the dependence of fatigue threshold on the R ratio (Elber, 1971; Suresh, xxx).

The proposed cohesive model does not involve an explicit representation of surface roughness or asperities of the crack surface. Rather, the model uses the parameter γ to capture decreases in damage possibly due to these effects. It was observed during the simulations that the crack retardation parameter γ was crucial for obtaining good agreement with a single set of parameters for both load ratios. This parameter γ can also capture other physical mechanisms for crack retardation, such as a plastic zone at the crack tip whose length scale is too small to be explicitly captured as plasticity of the bulk elements. Under plane strain assumptions, the estimated plastic zone size can be calculated as Anderson (2005)

$$r_p = \frac{1}{3\pi}\left(\frac{K_{Ic}}{\sigma_y}\right)^2, \tag{19}$$

which gives 1.3 mm plastic zone size for a CT specimen 9.1 mm thick. According to this calculation, the cohesive zone in our simulations is spanned by two elements. Further mesh refinement did not affect the results. This seems to indicate that indeed a mechanism other than plasticity is responsible for crack retardation, here captured by the damage decrease capability of the proposed cohesive model.

The results presented in this section can also be viewed in the form presented in the Paris law, namely crack growth rate versus stress intensity factor range. The following equation (ASTM, 2000) is used to reduce the test data and the simulation results to the information in Fig. 10:

$$\Delta K = \frac{\Delta P}{BW^{1/2}} f(a/W),$$

$$f\left(\frac{a}{W}\right) = \frac{\left(2+\frac{a}{W}\right)\left(0.886+4.64\left(\frac{a}{W}\right)-13.32\left(\frac{a}{W}\right)^2+14.72\left(\frac{a}{W}\right)^3-5.6\left(\frac{a}{W}\right)^4\right)}{\left(1-\frac{a}{W}\right)^{3/2}},$$

where a is the crack length, P is the tensile load range, B is the specimen thickness and W is the specimen width. As seen in the figure, the rate of crack growth and ΔK values predicted by the simulations match the test data. We observed that the measured crack speed oscillated considerably during the simulation. We suspect that this oscillation is an artifact of the method used to measure crack speed coupled with the discrete nature of our crack model. In particular, we measure the crack length by finding the farthest Gauss point along the crack path at which the opening displacement has reached its ultimate value (and hence the interface is traction-free). On some cycles, the damage variable κ can increase and yet not many Gauss points reach that zero-traction value. On these cycles, the measured crack length increment will be small. On the subsequent cycle, however, many Gauss points will reach the ultimate displacement simultaneously, yielding a large measured advance in crack length and hence a large crack speed. Our extrapolation method exacerbates this artifact because extrapolated cycles involve advancing the κ values but not the δ values. Although the crack speed measured on a cycle-by-cycle basis is oscillatory, the averaged crack speed over many cycles shows smooth and monotonically increasing behavior consistent with the test data.

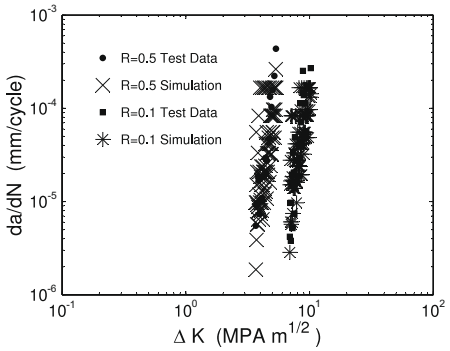

Fig. 10. da/dN vs. ΔK curve using the test data and simulations for $R = 0.1$ and $R = 0.5$ loading.

The question of existence of another triplet of parameters that could fit the experimental data was also investigated to check if the parameters α, β and γ are unique for a given material. A series of simulations were performed using higher values of the parameters. The observation from these simulations was that as the values were increased, crack growth first occurred at a later cycle. The crack started propagating much later than observed in the tests. Furthermore, the crack growth occurred at a much faster rate in order to attain the instability point at a cycle comparable to the tests. As a result, in order to match closely the initiation cycle, the instability cycle as well as the overall behavior in between these two events, the parameters appear to be unique.

Finally, the sensitivity of the simulation results to the damage evolution parameters was studied. Figs. 11–13 show the effect of varying the parameters α, β, and γ on the simulation results. As expected, the rate of damage accumulation and therefore the crack growth rate increases with α, and decreases with β and γ. Increasing values of both parameters β and γ enhance crack retardation by increasing the fatigue threshold and slowing damage accumulation during unloading, respectively.

6. Overload effect

Fatigue crack growth rates are well known to be decelerated by the application of overloads, which tend to cause an initial increase of the crack growth rate, followed by fast decrease before the final return to steady state crack propagation. The cause is usually attributed to plasticity induced crack closure, strain hardening, crack tip blunting, crack deflection, and/or branching depending on the toughness of the material. Wheatley et al. (1999) performed experiments on ductile 316 L steel, which indicated that overall crack retardation under plane stress conditions is related to strain hardening and residual compressive stresses in the plastic region of the overload. Plane stress simulations using the proposed model were performed on a CT specimen of width 40 mm and thickness 6 mm (Wheatley et al., 1998) with an initial crack 18 mm long. In the experiment, the pre-crack was initially a 12-mm blunt crack,

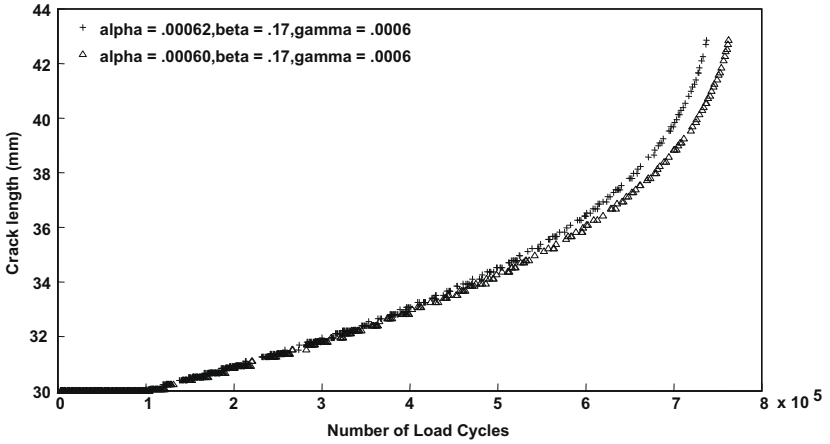

Fig. 11. Comparison of fatigue crack growth simulation results with varying α for $R = 0.5$ loading.

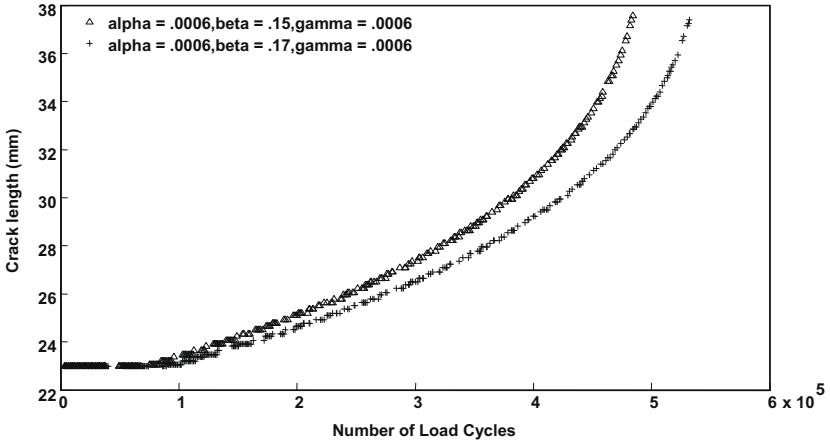

Fig. 12. Comparison of fatigue crack growth simulation results with varying β for $R = 0.1$ loading.

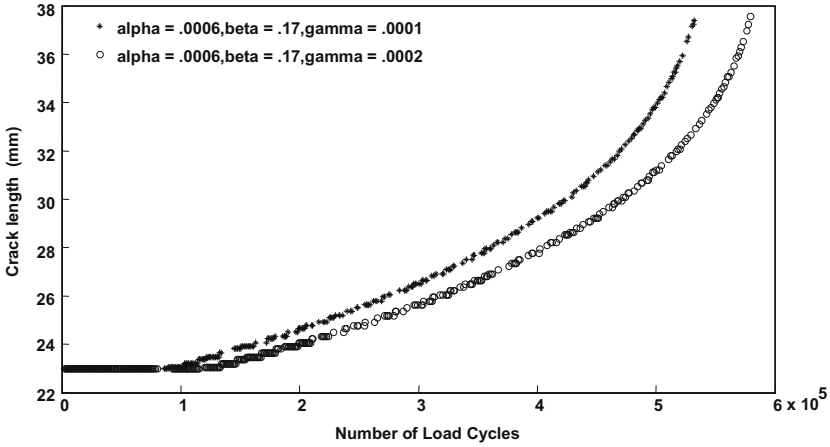

Fig. 13. Comparison of fatigue crack growth simulation results with varying γ for $R = 0.1$ loading.

which facilitated a 6-mm crack obtained with the application of high cycle fatigue loading. The applied loading ratio was $R = 0.1$ with a minimum load of 3 kN. An elastic-plastic material model with linear kinematic hardening was used to model the bulk material with parameters $E = 1.93$ GPa, $\nu = 0.33$, $\sigma_c = 588$ MPa, and $\sigma_y = 334$ MPa, as given in the experiment.

Fig. 14 shows simulation results for several single peak overloads applied early on (N=4000 cycles). Crack retardation is more pronounced when the overload is higher. The crack accelerates immediately following the overload but slows down within a few cycles and then reaches a minimum before eventually attaining the pre-load crack growth rate. The simulations closely match the experimental

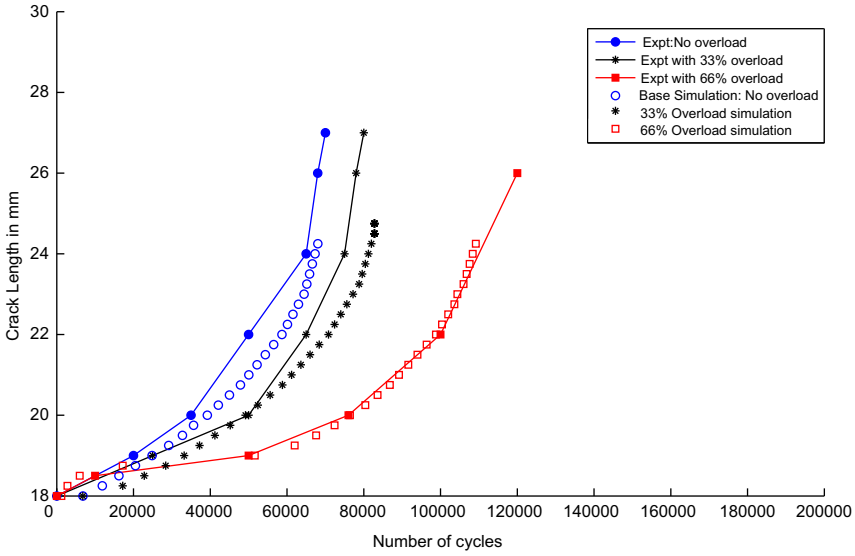

Fig. 14. Illustration of overload effect: crack retardation following application of a single peak overload increases with increasing value of the peak load.

results. The extrapolation scheme was applied during the constant amplitude portions of the loading, i.e., away from the overload. It was observed that using the extrapolation scheme soon after the application of the overload caused the finite element program to crash due to the sudden increase in the value of the damage variable in the process zone. Hence, cycle-by-cycle calculations were performed for a few cycles following the overload application.

Unlike in the cyclic loading of the aluminum alloy CT specimen described in the previous section, surface roughness and asperities do not seem to have significant effect on the crack growth rate in the present application. Based on fast scanning electron microscopy observations, Wheatley et al. (1999, 1998) suggest that strain hardening and residual stresses caused by plastic deformation due to the peak overload are responsible for crack retardation. To explain the immediate acceleration and subsequent retardation of crack growth, Wheatley et al. hypothesize a small fatigue damage zone ahead of the crack tip and argue that in their experiment crack closure was not a significant cause of the overload effect.

Compared to the aluminum alloy CT specimen, the plasticity zone causing crack retardation is much larger in this simulation due to the ductility of the material. Indeed, it is large enough to be represented well by plasticity of the elements in our mesh. (We confirmed the activity of the plasticity by observing a drastic change in the results when plasticity in our finite element analysis was disabled.) Thus, the cause of retardation is already captured by properties of the bulk elements, so there is no need for the γ parameter, which, as stated earlier, is intended to capture physical causes of crack retardation occurring at subgrid scales. Our FEM simulations corroborate this contention. Indeed setting γ equal to zero in the cohesive model made little difference in the crack retardation plots.

The physical interpretation is as follows: due to the sudden increase in load beyond the yield limit of the highly ductile material, strain hardening plasticity produces residual stresses in the plastic region, which envelopes the damage zone. These force the fatigue damage to be minimal and slow down the fatigue crack. Hence, even though the crack accelerates immediately following the application of the peak load due to a high value of K_{II}, the subsequent size of the damage zone ahead of the crack tip is reduced. The crack growth rate thereafter slowly increases as the size of the damage zone ahead of the crack tip increases to its pre-load value. In accordance with the theory presented in Wheatley et al. (1999, 1998), change in the yield stress of the material made a significant difference in the fatigue crack growth. As the ultimate stress was reduced towards a more brittle material, crack retardation was reduced to a point that it completely disappeared after the initial transient acceleration.

7. Summary

A damage-based cohesive zone model was developed for simulating fatigue under cyclic loading. The model introduces three material parameters that define the rate of evolution of a damage variable κ. Damage accumulation leads to eventual crack growth. The model has the feature that damage may also decrease, which leads to crack retardation. Damage decrease represents material "healing", as well as phenomenologically captures the different mechanisms that may lead to crack retardation. The three parameters have simple physical interpretations: they determine the rate of damage accumulation, the threshold value for accumulation of damage, and the rate of crack retardation. The admissible ranges of these parameters for well-posedness of the model were established.

The model was implemented within a cohesive interface finite element method. Algorithmic details for the evolution of damage were included in an appendix. Simulation results of fatigue tests of an aluminum alloy CT specimen at two loading ratios, $R = 0.1$ and $R = 0.5$, compare favorably with experimental results. A single set of parameters was determined that fit the tests at both load ratios. The ability of the model to capture crack retardation was crucial to this effect. Indeed, crack retardation was active in the $R = 0.1$ but not in the $R = 0.5$ simulation as was also observed in the experiment. A sensitivity study was carried out that determined the effect of these parameters on crack growth prediction.

The model was also used to predict crack retardation following a single peak overload. In this case crack retardation was due to the formation of residual stresses in the very large plastic zone of that material. This was adequately captured by a plasticity model in the bulk material.

Appendix. Detailed description of the algorithm

The value of the damage variable κ at each time step is obtained using the backward Euler method, which requires the value of κ from the previous time step and the derivative term as obtained from the evolution equations. Inputs to this algorithm are δ_n, δ_{n+1}

and κ_n, where subscripts n and $n+1$ correspond to time steps t_n and t_{n+1}, respectively. Outputs are κ_{n+1} and T_{n+1}. Define $\Delta\delta_{n+1} = \delta_{n+1} - \delta_n$.

If $\delta_n > \delta_u$
  $\kappa_{n+1} = 1$
  $T_{n+1} = 0$
  return
end
If $\Delta\delta_{n+1} > 0$
  $\alpha^* = \alpha$
else
  $\alpha^* = -\gamma$
end
Solve the following system of four equations for κ_{n+1}, $\Delta\kappa_{n+1}$, T_{n+1}, C_{n+1}:
  $\Delta\kappa_{n+1} = \alpha^*\kappa_{n+1}(T_{n+1} - \beta C_{n+1})(\Delta\delta_{n+1})$ (see (4)),
  $T_{n+1} = \frac{\sigma_c(1-\kappa_{n+1})\delta_{n+1}}{\kappa_{n+1}(\delta_u-\delta_c)+\delta_c}$ (see (1)),
  $C_{n+1} = \sigma_c(1-\kappa_{n+1})$ (see (3)),
  $\kappa_{n+1} = \kappa_n + \Delta\kappa_{n+1}$ (backward Euler).
  (Refer to the note below for the solution procedure.)
Let threshold $= \Delta\delta_{n+1}(T_{n+1} - \beta C_{n+1})$
If threshold > 0
  execute over-strength check (below)
  return
else
  $\kappa_{n+1} = \kappa_n$
  $T_{n+1} = F(\kappa_n)\delta_{n+1}$
  $C_{n+1} = C_n$
  execute over-strength check (below)
  return
end

The system of four equations described in this algorithm is solved using the following procedure. Observe that we can eliminate all the variables except κ_{n+1} with obvious substitutions. After this elimination, the following cubic equation is obtained:

$$a\kappa_{n+1}^3 + b\kappa_{n+1}^2 + c\kappa_{n+1} + d = 0 \tag{21}$$

where

$$a = \beta\sigma_c\alpha^*\Delta\delta_{n+1}(\delta_u - \delta_c),$$
$$b = -[(\delta_{n+1} - \beta\delta_c)\sigma_c\alpha^*\Delta\delta_{n+1} + \beta\sigma_c\alpha^*\Delta\delta_{n+1}(\delta_u - \delta_c) + (\delta_u - \delta_c)],$$
$$c = [\sigma_c\alpha^*\Delta\delta_{n+1}(\delta_{n+1} - \beta\delta_c) - \delta_c + \kappa_n(\delta_u - \delta_c)],$$
$$d = \kappa_n\delta_c.$$

Define a cubic function

$$\phi(\kappa) = a\kappa^3 + b\kappa^2 + c\kappa + d.$$

The cubic equation can be solved with the method of bisection. It is easy to see that $\phi(0) > 0$ and $\phi(1) < 0$. Therefore, there is at least one root of ϕ in $[0,1]$. Furthermore, the number of roots is odd, i.e., either one or three of the cubic's roots are in this interval. In fact, for $|\alpha^*|$ sufficiently small, there is only one root. The reason is that for $|\alpha^*|$ sufficiently small,

$$\phi'(1) \approx (\kappa_n - 1)(\delta_u - \delta_c) - \delta_c < 0.$$

Since ϕ' is a convex quadratic, if $\phi'(1) < 0$ then ϕ' has at most one root in $[0,1]$, which means that ϕ has at most one turning point in $[0,1]$. This makes it impossible for ϕ to have three roots in the interval.

Procedure over-strength check

If $\Delta\delta_{n+1} > 0$ and $T_{n+1} \geqslant C_{n+1}$
  $\kappa_{n+1} = \frac{\delta_{n+1}-\delta_c}{\delta_u-\delta_c}$
  $T_{n+1} = F(\kappa_{n+1})\delta_{n+1}$
end

This test ensures that the constraint $T \leqslant C(\kappa)$ holds at the end of the iteration.

References

Anderson, T.L., 2005. Fracture Mechanics: Fundamentals and Applications, third ed. Taylor and Francis, Boca Raton, FL.

ASTM, 2000. Standard test method for measurement of fatigue crack growth rates, p. E 647-99.

de Andres, A., Perez, J.L., Ortiz, M., 1999. Elastoplastic finite element analysis of three-dimensional fatigue crack growth in aluminum shafts subjected to axial loading. Int. J. Solids Struct. 36, 2231–2258.

Elber, W., 1971. The significance of fatigue crack closure. Am. Soc. Test. Mater. 486, 230–242.

Klein, P., Foulk, J., Chen, E., Wimmer, S., Gao, H., 2000. Physics-based modeling of brittle fracture: cohesive formulations and the application of meshfree methods. Technical Report SAND2001-8099, Sandia National Laboratories.

Lubliner, J., Oliver, J., Oller, S., Oñate, E., 1989. A plastic-damage model for concrete. Int. J. Solids Struct. 25 (3), 299–326.

Maiti, S., Geubelle, P.H., 2005. A cohesive model for fatigue failure of polymers. Eng. Fract. Mech. 72 (36), 691–708.

Maiti, S., Geubelle, P.H., 2006. Cohesive modeling of fatigue crack retardation in polymers: crack closure effect. Eng. Fract. Mech. 73 (1), 22–41.

Maiti, S., Shankar, C., Geubelle, P.H., Keiffer, J., 2006. Continuum and molecular modeling of fatigue crack retardation in self-healing polymers. J. Eng. Mater. Technol. 128 (4), 595–602.

Miller, K.J., 1991. Metal fatigue – past current and future. Proc. Inst. Mech. Eng. 205, 291–304.

Nguyen, O., Repetto, E.A., Ortiz, M., Radovitzky, R.A., 2001. A cohesive model of fatigue crack growth. Int. J. Fract. 110, 351–369.

Noroozi, A.H., Glinka, G., Lambert, S., 2008. Prediction of fatigue crack growth under constant amplitude loading and a single overload based on elasto-plastic crack tip stresses and strains. Eng. Fract. Mech. 75, 188–206.

Ortiz, M., Pandolfi, A., 1999. Finite-deformation irreversible cohesive elements for three dimensional crack propagation analysis. Int. J. Numer. Methods Eng. 44, 1267–1282.

Papoulia, K.D., Sam, C.-H., Vavasis, S.A., 2003. Time continuity in cohesive finite element modeling. Int. J. Numer. Methods Eng. 58 (5), 679–701.

Papoulia, K.D., Vavasis, S.A., Ganguly, P., 2006. Spatial convergence of crack nucleation using a cohesive finite element model on a pinwheel-based mesh. Int. J. Numer. Methods Eng. 67 (1), 1–16.

Paris, P.C., Erdogan, F., 1963. A critical analysis of crack propagation. Trans. ASME J. Basic Eng. 85, 528–534.

Paris, P.C., Gomez, M.P., Anderson, W.E., 1961. A rational theory of fatigue. Trends Eng. 13, 9–14.

Roe, K.L., Siegmund, T., 2001. An irreversible cohesive zone model for interface fatigue crack growth simulation. Eng. Fract. Mech. 70, 209–232.

Stephens, R.I. (Ed.), 1998. Fatigue and Fracture Toughness of A356-T6 Cast Aluminum Alloy, vol. SP-760. Society of Automotive Engineers, 400 Commonwealth Drive, Warrendale, PA 15096.

Suresh, S., 1998. Fatigue of Materials. Cambridge University Press.

Toohey, K.S., Sottos, N.R., Lewis, J.A., Moore, J.S., White, S.R., 2007. Self-healing materials with microvascular networks. Nat. Mater. 6, 581–585.

Ural, A., 2004. Advanced three-dimensional simulations and cohesive modeling of fatigue crack growth. Ph.D. thesis, Cornell University.

Ural, A. Papoulia, K.D., 2004. Modeling of fatigue crack growth with a damage-based cohesive zone model. In: Neittaanmäki, P. et al. (Eds.), Proceedings, European Congress on Computational Methods in Applied Sciences and Engineering, ECCOMAS 2004. Jyväskylä, Finland.

Wheatley, G., Hu, X.Z., Estrin, Y., 1999. Effects of a single tensile overload on fatigue crack growth in a 316 L steel. Fatigue Fract. Eng. Mater. Struct. 22 (12), 1041–1051.

Wheatley, G., Niefanger, R., Hu, X.Z., Estrin, Y., 1998. Fatigue crack growth in 316 L stainless steel. Key Eng. Mater. 145–149, 631–636.

White, S.R., Sottos, N.R., Geubelle, P.H., Moore, J.S., Kessler, M.R., Sriram, S.R., Brown, E.N., Viswanathan, S., 2001. Autonomic healing of polymer composites. Nature 409, 794–797.

Xu, X.-P., Needlemanm, A., 1994. Numerical simulations of fast crack growth in brittle solids. J. Mech. Phys. Solids 42 (9), 1397–1434.